Appl. Phys. B 81, 871–874 (2005)
DOI: 10.1007/s00340-005-2016-x

Applied Physics B
Lasers and Optics

G. GAY[1]
B. VIARIS DE LESEGNO[1,*]
R. MATHEVET[1]
J. WEINER[1,✉]
H.J. LEZEC[2,**]
T.W. EBBESEN[2]

Atomic fluorescence mapping of optical field intensity profiles issuing from nanostructured slits, milled into subwavelength metallic layers

[1] IRSAMC/LCAR, Université Paul Sabatier, 118 route de Narbonne, 31062 Toulouse, France
[2] ISIS, Université Louis Pasteur, 8 allée Gaspard Monge, 67083 Strasbourg, France

Received: 6 August 2005/Revised version: 11 September 2005
Published online: 22 October 2005 •

ABSTRACT We report on a direct spatial profile measurement of optical field intensity issuing from subwavelength slits flanked by periodic grooves and fabricated on a thin metallic layer. This type of structure is of interest for the manipulation of cold atoms by optical potentials near surfaces.

PACS 32.50.+d; 42.79.Gn

1 Introduction

Recently the use of micro- and nanostructures to generate magnetic and electro-magnetic fields useful for the manipulation of atoms near surfaces has been widely recognized and is developing rapidly [1]. The interest in optical fields is twofold: first, field gradients of unconventional size and shape can be tailored to capture, trap, and transport atoms, either singly [2] or collectively [3]. Secondly, tapered optical fiber structures can be designed to integrate the capture, and precise placement of atoms on surfaces in controlled deposition [4] or for experiments in quantum information [5]. Several research groups are actively investigating the tailoring of these fields based on refraction [6], reflection [7], and diffraction [8]; and because the fields of interest are in the near- or intermediate field regime, it is important to develop methods for directly measuring and mapping field or intensity distributions. The use of leakage radiation from metal film/glass interfaces [9] and organic dye molecules [10] as fluorescence markers have been reported.

Here we describe the use of atom beam fluorescence to measure a spatial profile of the highly confined and collimated optical field issuing from a subwavelength slit milled by a focused ion beam (FIB) into a thin metallic layer deposited on a glass substrate. This technique measures optical intensity distributions in the far field; and therefore, unlike near-field scanning tip microscopies, is subject to diffraction-limited spatial resolution. It has, however, the advantage of rapidly producing a quantitative global intensity map since the relation between gas-phase fluorescence and atom photoexcitation are simple and well-understood. It also has some advantages over the use of dye molecule films: bleaching or optical pumping into dark states can be avoided and the fluorescence rate is not a sensitive function of the atom–surface distance, at least to within the 5 μm resolution of these measurements. Subwavelength slits flanked by periodically spaced grooves in the metal layer have been shown to produce propagating light, highly confined transversely and "beaming" perpendicular to the structure plane [11–13]. The profiling technique reported here enables the investigation of the beaming intensity distribution in the far field as a function of groove parameters, their number and spacing.

2 Apparatus description

Figure 1 shows a schematic diagram of the experiment. A thermal oven source heats a Cs metal reservoir to ∼ 370 K. Through an output nozzle, the Cs atomic beam effuses through a long narrow tube 36 mm in length, 1.6 mm diameter. The long aspect ratio of the nozzle acts as a mechanical precollimator for the atom beam that subsequently passes through a zone of transverse optical molasses [14]. Cooling of the atomic transverse velocity components results in a very "bright" [15] Cs atom beam along the z direction, highly collimated to a divergence < 1 mrad. The optical molasses zone also leads to some slowing and cooling of the longitudinal velocity components as can be seen in Fig. 2. The collimated atom flux then passes in front of and parallel to a planar subwavelength slit structure, illuminated on the back side by a focused laser and from which issues on the front side a highly collimated light field propagating along x, perpendicular to the atom flux. The laser beam is linearly polarized perpendicular to the long axis of the slit.

The subwavelength slit structure is shown in Fig. 3. It consists of a silver layer 415 nm thick deposited on a glass

✉ Fax: 33 (0) 5 6155 8317, E-mail: jweiner@irsamc.ups-tlse.fr
*Present address: Laboratoire Aimé Cotton, Campus d'Orsay, 91405 Orsay, France
**Present address: Thomas J. Watson Laboratories of Applied Physics, California Institute of Technology, Pasadena, California 91125 USA

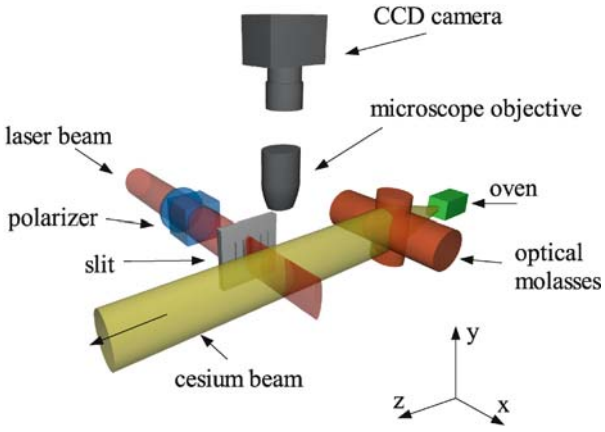

FIGURE 1 Atomic cesium beam effuses from a thermal oven and is collimated by transverse optical molasses cooling to a divergence of less than 1 mrad with a forward flux density of $\simeq 10^{12}\,\mathrm{cm}^{-2}\,\mathrm{s}^{-1}$. A monomode cw laser beam, tuned to the Cs D2 resonance line, impinges on the back plane of the nanostructured slit. Highly collimated "beamed light" propagates from the front plane of the slit and crosses the atomic beam at right angles. The resulting fluorescence profile is imaged by the microscope objective onto a CCD camera with 5 μm per pixel resolution

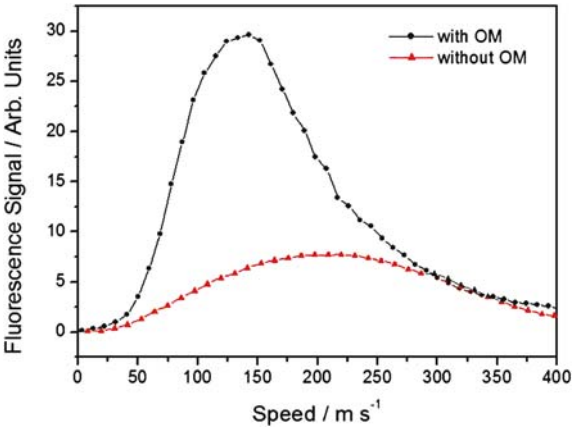

FIGURE 2 Cs beam longitudinal velocity distribution with and without the collimating optical molasses present. The narrowing of the longitudinal distribution clearly shows evidence of cooling in the presence of the transverse optical molasses

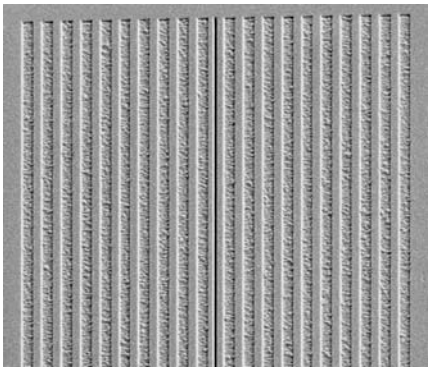

FIGURE 3 Scanning electron microscope image of the nanostructured silver layer. The layer is 415 nm thick and deposited on a glass substrate. The central slit is 100 nm wide and 50 μm long, flanked on each side by 10 grooves separated with a period of 830 nm. The groove dimensions are 460 nm width and 130 nm depth

substrate. FIB milling is used to fabricate a central slit (100 nm width, 50 μm length) flanked by 10 grooves on each side. The groove period is 830 nm and the groove width and depth (460 nm and 130 nm, respectively) have been optimized for maximum intensity far-field "beaming" at the Cs resonant wavelength of 852 nm.

The laser illuminating the slit from the back is tuned over the $\mathrm{Cs}^2S_{1/2} \leftrightarrow {}^2P_{3/2}$ transition producing a fluorescence profile of the intensity distribution issuing from the front side of the planar structure. With the laser tuned to the center of the resonance line, we have measured the fluorescence intensity as a function of laser intensity to ensure that the excitation is always in the weak linear regime and does not approach saturation. The fluorescence is collected by a microscope objective (N.A. 0.28, resolving power 1 μm) mounted above the plane; and, after passing through a polarizing beam splitter to filter scattered light from atomic fluorescence, is focused onto a CCD camera. The depth of focus was independently measured to ensure that light collection over the 50 μm slit length did not degrade the spatial resolution of the optical system. The overall profile resolution is 5 μm per pixel.

3 Profile analysis

Figure 4 shows a spatial and intensity profile issuing from the slit structure of Fig. 3 with 10 grooves on each side, and Fig. 5 shows the profile for a similar structure with 30 grooves. With the 30-groove structure the divergence of the "beaming" is reduced by about a factor 2.5 and the intensity increased by about 40%. Figure 6 summarizes the results for the measured angular beam divergences from structures fabricated with 10 to 30 grooves on each side of the slit. In order to infer the true width and divergence of the propagating field from the fluorescence map, several factors must be taken into account. The most important of these is the effective Doppler broadening due to the light beaming direction $\boldsymbol{k}(\boldsymbol{r})$ and longitudinal velocity distribution $\boldsymbol{v}_\parallel$ in the atomic beam. The differential fluorescence rate $\mathrm{d}\varrho^*(\boldsymbol{r})$, proportional to the atom excited state distribution at fixed laser frequency ω_L and velocity $\boldsymbol{v}_\parallel$ is given by,

$$\mathrm{d}\varrho^*(\boldsymbol{r}) \propto \frac{\Omega_0^2(\boldsymbol{r})/4}{\left\{\begin{array}{l}(\Delta\omega - \boldsymbol{k}(\boldsymbol{r})\,\boldsymbol{v}_\parallel)^2 + \\ \Gamma^2/4 + \Omega_0^2(\boldsymbol{r})/2\end{array}\right\}} f(\boldsymbol{v}_\parallel)\mathrm{d}\boldsymbol{v}_\parallel \mathrm{d}\omega_\mathrm{L} \quad (1)$$

where $\hbar\Omega_0 = \boldsymbol{\mu}\,\boldsymbol{E}$ is the dipole interaction energy between the atomic transition moment $\boldsymbol{\mu}$ and the optical field $\boldsymbol{E}$, $\Delta\omega = \omega_\mathrm{L} - \omega_0$ is the laser detuning from the optical transition resonance frequency ω_0, Γ the natural width of the atomic transition, and $f(\boldsymbol{v}_\parallel)\mathrm{d}\boldsymbol{v}_\parallel$ the atom beam velocity distribution. The term $\Omega_0^2(\boldsymbol{r})$ is proportional to the intensity of the "beaming" field propagating from the slit structure. The factor $\boldsymbol{k}(\boldsymbol{r})\,\boldsymbol{v}_\parallel$ is the effective first-order Doppler detuning arising from the far-field divergence of the light beam propagation vector $\boldsymbol{k}$ intersecting an atomic beam velocity component $\boldsymbol{v}_\parallel$. The spatial fluorescence map proportional to the intensity distribution of the emitting nanostructure, is given by,

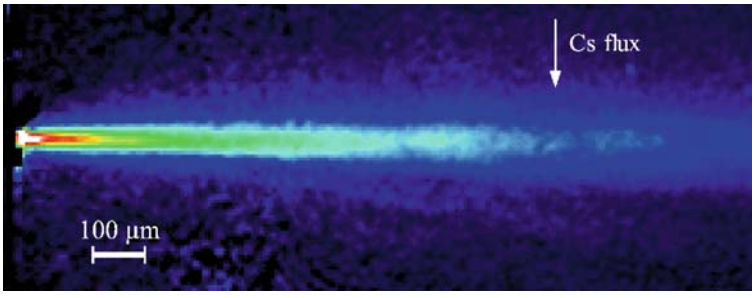

FIGURE 4 Atomic fluorescence map $\varrho^*(\boldsymbol{r})$ of the optical intensity spatial distribution issuing from the nanostructured slit flanked by 10 grooves on each side. The exciting laser is scanned over the Cs D2 resonance line. The intensity scale is normalized to the maximum. Each pixel of the CCD image corresponds to 5 μm

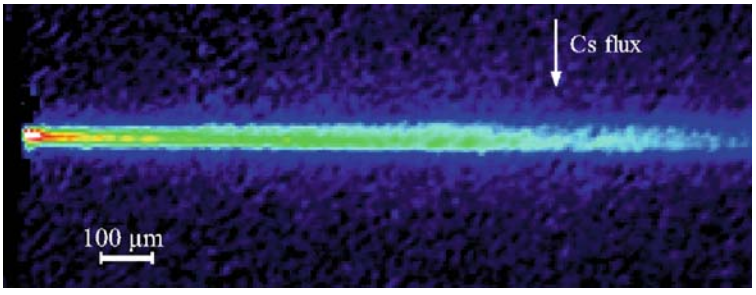

FIGURE 5 Atomic fluorescence map $\varrho^*(\boldsymbol{r})$ of the optical intensity spatial distribution issuing from the nanostructured slit flanked by 30 grooves on each side. Note the marked decrease in divergence compared to the structure with ten grooves. The intensity scale is normalized to the maximum. Each pixel of the CCD image corresponds to 5 μm

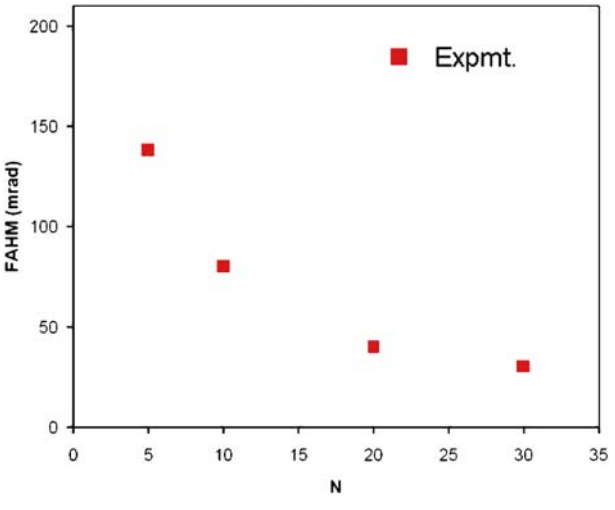

FIGURE 6 Measured angular divergence (mrad) as a function of the number N of flanking grooves for the slit structures of Fig. 3

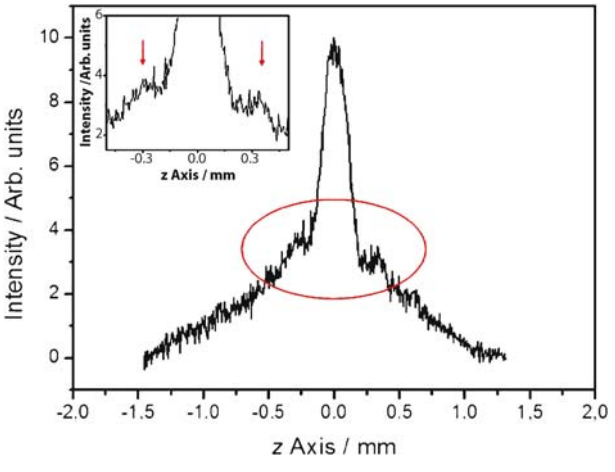

FIGURE 7 Transverse cut (along z axis) of the light beam issuing from a slit flanked by 20 grooves on each side of the same pitch, width, and depth as shown in Fig. 3. The cut was measured at a distance of 5 mm along the x axis, perpendicular to the slit structure. The *inset* shows a detail of the supernumerary structure, indicated by *arrows*, adjacent on each side of the main light beam

$$\varrho^*(\boldsymbol{r}) \propto \int \mathrm{d}\omega_\mathrm{L} \int \mathrm{d}\boldsymbol{v}_\parallel \frac{\Omega_0^2(\boldsymbol{r})/4}{\left\{\begin{array}{c}(\Delta\omega - \boldsymbol{k}(\boldsymbol{r})\,\boldsymbol{v}_\parallel)^2 + \\ \Gamma^2/4 + \Omega_0^2(\boldsymbol{r})/2\end{array}\right\}} f(\boldsymbol{v}_\parallel)$$

$$\propto \Omega_0^2(\boldsymbol{r}) \times \int_0^{+\infty} \mathrm{d}\omega_\mathrm{L} \int_0^{+\infty} \mathrm{d}\boldsymbol{v}_\parallel \frac{1/4}{\left\{\begin{array}{c}(\omega_\mathrm{L} - \omega_0')^2 + \\ \Gamma^2/4\end{array}\right\}} f(\boldsymbol{v}_\parallel) \tag{2}$$

$$\propto \Omega_0^2(\boldsymbol{r}) \frac{\pi}{4\Gamma} \int_0^{+\infty} f(\boldsymbol{v}_\parallel)\mathrm{d}\boldsymbol{v}_\parallel \tag{3}$$

where in (2) we have defined $\omega_0' = \omega_0 - \boldsymbol{k}(\boldsymbol{r})\,\boldsymbol{v}_\parallel$, the resonant frequency for an atom excited by beaming light in direction $\boldsymbol{k}(\boldsymbol{r})$ at fixed $\boldsymbol{v}_\parallel$. The last term in the denominator $\Omega_0^2(\boldsymbol{r})/2$ has been dropped because under our experimental conditions this term is always small compared to the sum of the others. In the experiment the atomic fluorescence is integrated while the laser frequency ω_L is tuned over the entire Doppler distribution, and (2) and (3) show that the integrated fluorescence profiles $\varrho^*(\boldsymbol{r})$, of Figs. 4 and 5 are directly proportional to the spatial intensity distribution of the field, $\Omega_0^2(\boldsymbol{r})$, emitted by the structured slits. The integrated velocity distribution in (3) (such as the one shown in Fig. 2) simply contributes a constant factor to the proportionality between atom density and the field intensity.

Another factor limiting the vertical resolution in Figs. 4 and 5 is the atomic fluorescence lifetime, $\simeq 30$ ns for Cs. As the fluorescing atoms exit the optical field with a peak velocity $\simeq 150\,\mathrm{ms}^{-1}$, (see Fig. 2) they will travel $\simeq 4.5$ μm before relaxing to the ground state. This fluorescence time delay is not readily discernable in Figs. 4 and 5 because the image resolution on the CCD camera is 5 μm per pixel.

The light emanating from these slit structures is not always spatially uniform. Figure 7 shows a profile cut along the z axis of a light beam issuing from the same type of slit structure as shown in Fig. 3 but with 20 grooves on each side. The clear evidence of shoulders indicates that the principal beaming light is flanked by side lobes. A study of these supernumerary structures will be presented in a future publication.

Other forms and arrangements of structures can be readily fabricated. For example, grooves that are not evenly spaced but regularly increase their pitch may serve to focus light in front of the slit rather than to simply collimate it. Two dimensional structures such as round holes surrounded by concentric rings will give rise to collimated and focused light in two dimensions. The optical potential gradients generated by these structures can be used for cold atom trapping and manipulation. The structures themselves can be fabricated in one- or two-dimensional arrays, either on glass substrates or as free standing metallic membranes.

4 Summary of results

We have reported here a new technique for mapping the spatial and intensity distribution of fields emanating from nanostructured subwavelength slits in thin metallic layers deposited on transparent substrates. These fields result from the superposition of a weak field component directly transmitted through the slit and field components due to the excitation of evanescent surface waves originating at the slit and their subsequent reemission from the flanking grooves. We have observed that the divergence of the resulting "beaming" light decreases from 80 mrad for a 10-groove structure to 30 mrad for 30-groove structure and that supernumerary lobes sometimes appear adjacent to the main beam. Further systematic studies of divergence and intensity as a function of groove number and distance from both slits and holes should help to characterize the properties of the surface waves launched from the subwavelength structure.

ACKNOWLEDGEMENTS This work was supported in part by the European Community's IST Programme under contract IST-2001-32264, Région Midi-Pyrénées under contract SFC/CR 02/22, under the ACI Nanosciences Nanotechnologies Programme of the Ministère de l'Education Nationale, de l'Enseignement Supérieur et de Recherche.

REFERENCES

1 R. Folman, P. Krüger, J. Schmiedmayer, J. Denschlag, C. Henkel, Adv. At. Mol. Opt. Phys. **48**, 263 (2003) and references cited therein
2 S.B. Hill, J.J. McClelland, Appl. Phys. Lett. **82**, 3128 (2003)
3 D. Rychtarik, B. Engeser, H.-C. Nägerl, R. Grimm, Phys. Rev. Lett. **92**, 173003-1 (2004)
4 I. Dotsenko, W. Alt, M. Khudaverdyan, S. Kuhr, D. Meschede, Y. Miroshnychenko, D. Schrader, A. Rauschenbeutel, Phys. Rev. Lett. **95**, 033002 (2005)
5 J. Mompart, K. Eckert, W. Ertmer, G. Birkl, M. Lewenstein, Phys. Rev. Lett. **90**, 147901-1 (2003)
6 R. Dumke, M. Volk, T. Müther, F.B.J. Buchkremer, G. Birkl, W. Ertmer, Phys. Rev. Lett. **89**, 097903-1 (2002)
7 E.A. Hinds, private communication
8 G. Lévêque, C. Meier, R. Mathevet, C. Robilliard, J. Weiner, C. Girard, J.C. Weeber, Phys. Rev. **65**, 053615-1 (2002)
9 A.L. Stepanov, J.R. Krenn, H. Ditlbacher, A. Hohenau, A. Drezet, B. Steinberger, A. Leitner, F.R. Aussenegg, Appl. Phys. Lett. **30**, 1524 (2005)
10 H. Ditlbacher, J.R. Krenn, N. Felidj, B. Lamprecht, G. Schider, M. Salerno, A. Leitner, F.R. Aussenegg, Appl. Phys. Lett. **80**, 404 (2002)
11 L. Martín-Moreno, F.J. García-Vidal, H.J. Lezec, A. Degiron, T.W. Ebbesen, Phys. Rev. Lett. **90**, 167401-1 (2003)
12 H.J. Lezec, A. Degiron, E. Devaux, R.A. Linke, L. Martín-Moreno, F.J. García-Vidal, T.W. Ebbesen, Science **297**, 820 (2002)
13 F.J. García-Vidal, H.J. Lezec, T.W. Ebbesen, L. Marín-Moreno, Phys. Rev. Lett. **90**, 213901-1 (2003)
14 An introduction to the physics of optical cooling and trapping can be found in two special issues of the *Journal of the Optical Society of America* B. These are: J. Opt. Soc. Am. B, **6**, No. 11 (1985) and J. Opt. Soc. Am B, **6** No. 11 (1989)
15 W. DeGraffenreid, Y-M. Liu, J. Ramirez-Serrano, J. Weiner, Rev. Sci. Instr. **70**, 3668 (2000)